Journal Title
XX(X):1–8
©The Author(s) 0000
Reprints and permission:
sagepub.co.uk/journalsPermissions.nav
DOI: 10.1177/ToBeAssigned
www.sagepub.com/
SAGE

An optimal orbit design for LISA

Yaguang Yang[1]

Abstract

The ESA/NASA joint LISA (laser interferometer space antenna) mission is designed to detect gravitational waves to perform gravitational astronomy. A key mission requirement is the maintenance of a three-spacecraft constellation in a near-equilateral triangular configuration with a prescribed inter-spacecraft separation. Existing approaches have addressed this problem using simplified dynamical models to enhance tractability; however, the resulting solutions are generally suboptimal with respect to the true system dynamics. In this paper, a precise nonlinear model based on exact nonlinear Keplerian orbit equations is developed. The orbit design problem is consequently formulated as a nonlinear, nonconvex optimization problem. An efficient arc-search interior-point method is employed to address the challenging optimization problem. Numerical results demonstrate that the obtained optimal solution enforces strict agreement between the mean formation distance and the prescribed value. Moreover, the proposed methodology is readily extensible to other optimal orbit design problems formulated using higher-fidelity dynamical models.

Keywords

LISA, formation fly, optimal orbit design

Introduction

LISA is an ESA/NASA mission aimed at sensing low-frequency gravitational waves, with a measurement band spanning 0.1mHz to 1Hz. The mission employs a formation-flying configuration consisting of three spacecraft, each in a heliocentric orbit. Collectively, the spacecraft form the vertices of an approximately equilateral triangle that evolves over time. The designed distance between any pair of spacecraft is 2.5 million kilometers at any time. However, since each spacecraft follows its independent heliocentric trajectory governed by the nonlinear Keplerian orbital equations, the inter-spacecraft distances exhibit time-dependent variations about the prescribed value[1]. These variations induce Doppler shifts and breathing angles that affect the interferometers' measurement[2,3]. Minimizing such distance variations is therefore critical to satisfying engineering constraints, including the motion range of the Optical Assembly Tracking Mechanism and the bandwidth limitations of the LISA phasemeter.

The optimal orbit design problem—minimizing distance variations about the nominal triangular configuration—is inherently challenging due to the nonlinear and nonconvex nature of the constraints of Keplerian equations, which precludes closed-form analytic solutions. Consequently, various approximations have been considered by researchers[1–5] so that simplified linear or quadratic problems based on approximate models can be solved. For example, Hughes[5] explored all six Keplerian elements within a simplified framework; De Marchi et al[2] employed a linearized model (a first-order approximation model)[6] to reduce the distance deviations among all pairs of spacecraft; similarly, Dhurandhar et al[1] used a first-order approximation model to demonstrate that the three-spacecraft constellation maintains an approximate equilateral triangle configuration (we will refer to this orbit as the DNKV orbit); Nayak et al[3] introduced a second-order approximation model (we will refer to this orbit as the NKDV orbit) to improve the solution of Dhurandhar et al. Although these approaches do not produce truly optimal solutions, they provide valuable insight into desirable orbit characteristics. Furthermore, the solution obtained by Nayak et al[3] has been adopted as a baseline* for a higher-fidelity LISA model[7], as implemented by Bayle et al[8].

In this paper, we propose an optimal LISA orbit design that leverages high-fidelity nonlinear Keplerian orbit equations to obtain an accurate solution, assuming that the Sun provides the primary gravitational influence in the two-body model. Rather than pursuing an analytic solution, we adopt a numerical approach to achieve high accuracy. To facilitate this, we exploit all available physical and geometric constraints to simplify the problem without compromising model fidelity. In

[1]Goddard Space Flight Center, NASA

Corresponding author:
Yaguang Yang, NASA Mission Engineering and Systems Analysis Division, 8800 Greenbelt Rd, Greenbelt, 20771 MD, USA.
Email: yaguang.yang@verizon.net

*This solution serves as an initial guess for optimizing a full nonlinear model that includes multiple gravitating bodies in the solar system[7]. For nonlinear and nonconvex optimization problem (which may admit multiple local optimizers), a high-quality initial guess is essential.

particular, implicit relationships are used to eliminate dependent and irrelevant variables, retaining only a minimal set of independent variables, thereby enabling an efficient and precise numerical solution. According to the analysis of Dhurandhar et al[1], the virtual center of the triangular configuration formed by the three LISA spacecraft follows a circular heliocentric orbit located approximately 20^o degrees behind the Earth[†]. This configuration implies that all three spacecraft share the same orbital period T as the Earth; consequently, their semi-major axes a are also identical, as given by Yang[9]. Moreover, the orbits of the three spacecraft are essentially identical, with relative rotations of 120^o within the Earth's orbital plane in a heliocentric frame. Consequently, the right ascensions of the ascending nodes differ by 120^o and can be fixed, while the arguments of perigee are also fixed. Since the orbital period T is known and identical for all three spacecraft, their mean motions are likewise fixed[9]. Therefore, among the six Keplerian elements, only the eccentricity e and inclination i influence the magnitude of the inter-spacecraft distance variation. As a result, the problem can be simplified by considering only these two parameters without compromising model accuracy in determining the optimal solution.

On the other hand, employing the full nonlinear Keplerian dynamics while optimizing over both eccentricity and inclination enables exploration of a broader and more physically accurate solution space, which may produce improved solutions relative to simplified models, although global optimality and global convergence are not guaranteed due to the problem's nonlinear and nonconvex nature[10,11]. Since no existing nonlinear optimization algorithm can guarantee convergence to a solution for all nonlinear optimization problems, we adopt a recently developed arc-search optimization method of Yang[12] due to its computational efficiency and established convergence properties[12,19]. The algorithm is implemented to solve the optimal LISA orbit design problem, and the results are compared with previously obtained solutions. For a fair comparison, we adopt the same assumptions used in relevant literature[1,3–5], namely that the Sun is the only gravitationally attracting body in the solar system. When additional perturbations, such as gravitational influences from other celestial bodies and variations in the spacecraft–Sun distance, are included, a purely numerical optimization approach becomes necessary for the resulting higher-fidelity problem. Therefore, the proposed state-of-the-art nonlinear optimization method can be extended to such higher-fidelity settings (a direction for future work), whereas the ad hoc methods of Dhurandhar et al and Nayak et al[1,3] are not readily applicable.

State-of-the-art for Keplerian LISA orbit designs

Let the barycentric frame with coordinates (X,Y,Z) for spacecraft 1 be defined (see Figure 1) as follows. The ecliptic plane coincides with the X–Y plane,

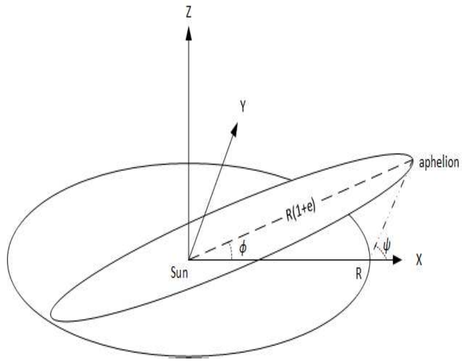

Figure 1. The geometry of the LISA spacecraft orbit with respect to the ecliptic plane.

and a circular reference orbit of radius $R = 1AU = 1.49597870 \times 10^8$ km is centered at the Sun[13]. For an elliptical orbit with its true focus at the Sun (the true focus is defined in Wie[14]), let a denote the semi-major axis, e the eccentricity, and E the eccentric anomaly. Following the discussion in Dhurandhar et al[1], we first consider a single spacecraft orbit and subsequently construct the remaining spacecraft orbits. In accordance with Dhurandhar et al[1], we choose $t = 0$ at the time when the spacecraft is at aphelion, located along the +X axis. This coordinate convention differs from that used in many standard references, and the chosen initial condition leads to sign differences in several expressions below. The orbit geometry is illustrated in Figure 1. According to Vallado[13] and Dhurandhar et al[1], the following relations hold.

$$X = a(\cos(E) + e), \quad Y = a\sqrt{1 - e^2}\sin(E). \tag{1}$$

Let $\mu = 1.32712428 \times 10^{11} km^3/s^2$ denote the heliocentric gravitational constant[?] vallado01 and $\Omega = \sqrt{\mu/a^3}$ be the mean motion, then Kepler's equation is given by Vallado[13]

$$E + e\sin(E) = \Omega t, \tag{2}$$

where Ωt is the mean anomaly and E is the eccentric anomaly of the spacecraft. Let the orbit of spacecraft 1 be obtained by rotating the elliptical orbit about the $-Y$-axis by an inclination angle i, such that its maximum Z-coordinate at $t = 0$ is lie in the positive X-direction. At this reference point, $E = 0$, $X = a(1 + e)\cos(i)$, $Y = 0$, and $Z = a(1 + e)\sin(i)$. In general, the

[†]To mitigate the Earth's gravitational perturbations on the LISA formation (thereby improving formation stability), the spacecraft should ideally be placed far from the Earth. However, practical considerations—such as fuel and power consumption, as well as communication delay and telemetry constraints—favor a closer proximity. A 20^o trailing configuration represents a compromise between these competing requirements.

orbit can be expressed as

$$X_1(E) = a(\cos(E) + e)\cos(i) \tag{3a}$$
$$Y_1(E) = a\sqrt{1 - e^2}\sin(E) \tag{3b}$$
$$Z_1(E) = a(\cos(E) + e)\sin(i) \tag{3c}$$

where E is implicitly related to the time t through (2). Let the orbit of spacecraft 2 be obtained by rotating the orbit of spacecraft 1 about the Z-axis by $\frac{2}{3}\pi$ and the orbit of spacecraft 3 be obtained by rotating the orbit of spacecraft 1 about the Z-axis by $\frac{4}{3}\pi$. Then, their orbits can be expressed as

$$X_k = X_1(E_k)\cos\left(\frac{2\pi}{3}(k-1)\right) - Y_1(E_k)\sin\left(\frac{2\pi}{3}(k-1)\right), \tag{4a}$$

$$Y_k = X_1(E_k)\sin\left(\frac{2\pi}{3}(k-1)\right) + Y_1(E_k)\cos\left(\frac{2\pi}{3}(k-1)\right), \tag{4b}$$

$$Z_k = Z_1(E_k), \tag{4c}$$

where $k = 1, 2, 3$, and E_k depends implicitly on time t through Kepler's equations

$$E_k + e\sin(E_k) = \Omega t - (k-1)\frac{2\pi}{3}. \tag{5}$$

We will use this coordinate system throughout the paper. Let $\ell = 2,500,000$ km denote the desired distance between any two spacecraft in the constellation, and define $\alpha = \ell/2R$. In the remainder of the paper, we first review two existing orbit designs, then propose an optimal orbit design, and compare their deviations from the desired inter-spacecraft distance.

DNKV orbit

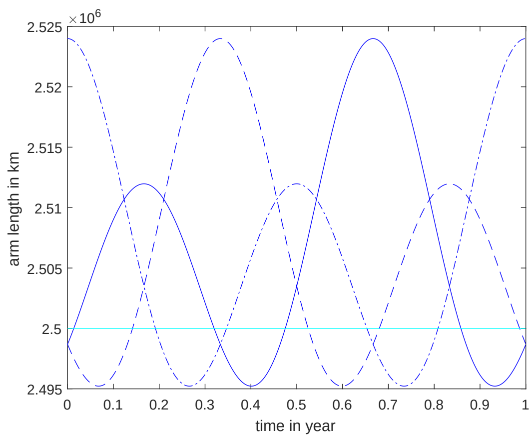

Figure 2. Inter-spacecraft distances over one orbital period (one year) for the DNKV orbit, using 629 sampling points.

In view of Figure 1, let ψ be the angle between the X axis and the line segment joining the aphelion of spacecraft 1 to the intersection of the X axis with the reference circular orbit on the ecliptic plane; setting $\psi = \pi/3$, Dhurandhar et al[1] have shown that

$$\tan(i) = \frac{\alpha}{1 + \alpha/\sqrt{3}}, \tag{6a}$$

$$e = \left(1 + \frac{2\alpha}{\sqrt{3}} + \frac{4\alpha^2}{3}\right)^{1/2} - 1, \tag{6b}$$

and that the spacecraft constellation evolves approximately as three vertices of a moving equilateral triangle (i.e., the distances between any pair of spacecraft are not strictly constant), with its center following the reference circular orbit. For given values of α and a, the corresponding eccentricity e and inclination i can be determined. Using Eqs. (3), (4), and (5), the orbits of the three spacecraft can then be obtained. The inter-spacecraft distances are illustrated in Figure 2. The horizontal line represents the nominal (desired) separation between each pair of spacecraft. The solid, dashed, and dash-dotted curves correspond to the distance variations between spacecraft pairs 1&2, 1&3, and 2&3, respectively. Figure 2 closely resembles the result reported by Dhurandhar et al[1], with a peak-to-peak variation of approximately 28,820 km. However, the inter-spacecraft separations for all pairs are required to remain close to the nominal value of 2.5×10^6 km.

NKDV orbit

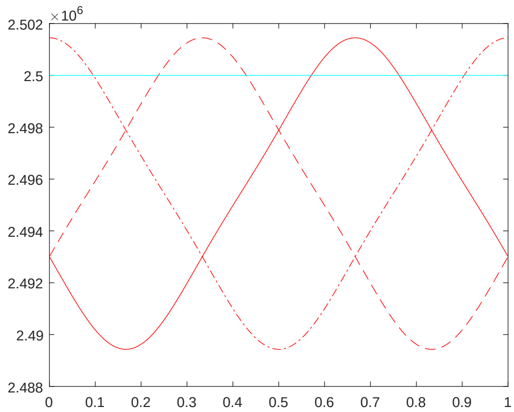

Figure 3. Inter-spacecraft distances over one orbital period (one year) for the NKDV orbit, using 629 sampling points.

To reduce the variation in inter-spacecraft distances, Nayak et al[3] allow the angle ψ to be adjusted about $\pi/3$, i.e., $\psi = \pi/3 + \delta$. Within a second-order approximation, the optimal value is found to be $\delta = \frac{5}{8}\alpha$, and the following relations hold.

$$\tan(i) = \frac{2}{\sqrt{3}} \frac{\alpha\sin(\pi/3 + \delta)}{[1 + \frac{2}{\sqrt{3}}\alpha\cos(\pi/3 + \delta)]}, \tag{7a}$$

$$e = \left(1 + \frac{4\alpha^2}{3} + \frac{4\alpha}{\sqrt{3}}\cos(\pi/3 + \delta)\right)^{1/2} - 1. \tag{7b}$$

Given α, δ, and a, the corresponding eccentricity e and inclination i can be determined. Using Eqs. (3), (4), and (5), the orbits of the three spacecraft can then be obtained. The inter-spacecraft distances predicted by the second-order model are shown in Figure 3. In this figure, the horizontal line represents the nominal (desired) separation between each spacecraft pair. The solid, dashed, and dash-dotted curves correspond to the distance variations between spacecraft pairs 1&2, 1&3, and 2&3, respectively. Notably, the peak-to-peak variation in the inter-spacecraft distance for the second-order (NKDV) design is approximately 12,000 km, representing a significant improvement over the DNKV design (28,820 km). However, the mean inter-spacecraft distances deviate from the nominal value of 2.5×10^6 km, consistent with the results reported by Martens and Joffre[7].

The optimal orbit design

The optimal orbit design is obtained using an arc-search technique for interior-point methods.

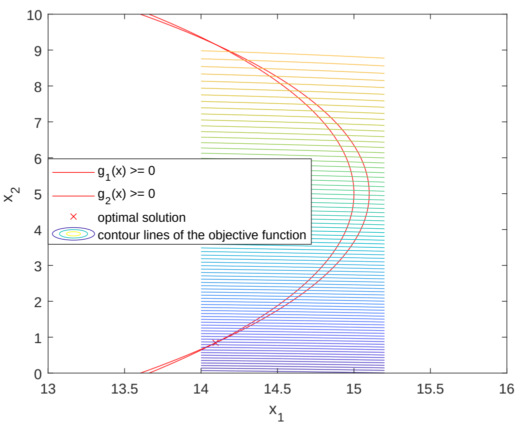

Figure 4. The constraints of HS-19.

An arc-search infeasible interior-point algorithm

The LISA orbit design problem can be formulated as a general nonlinear optimization problem of the form

$$\begin{array}{rcl} \min & : & f(\mathbf{x}) \\ \text{s.t.} & : & \mathbf{h}(\mathbf{x}) = \mathbf{0} \\ & & \mathbf{g}(\mathbf{x}) \geq \mathbf{0} \end{array} \quad (8)$$

where $f : \mathbb{R}^n \to \mathbb{R}$ denotes a linear or nonlinear objective function, $\mathbf{h}(\mathbf{x}) = \mathbf{0}$ represents m linear and/or nonlinear equality constraints, and $\mathbf{g}(\mathbf{x}) \geq \mathbf{0}$ represents p linear and/or nonlinear inequality constraints[‡].

Among the available solution approaches, the infeasible interior-point method has gained significant popularity for solving such nonlinear and nonconvex optimization problems[12,16]. The key idea is to start with an initial point $\mathbf{x}^0$ that satisfies the inequality constraints (i.e., an interior point) but may violate the equality constraints (i.e., an infeasible point), since solving the nonlinear system of equations $\mathbf{h}(\mathbf{x}) = \mathbf{0}$ exactly can be computationally expensive. As the iteration sequence $\{\mathbf{x}^k\}$ progresses toward the optimal solution $\mathbf{x}^*$, the iterates are driven toward feasibility, ultimately satisfying both equality and inequality constraints. Traditional optimization methods typically rely on a line search to determine a suitable step at each iteration. However, this approach can be inefficient when dealing with nonlinear and nonconvex constraints, as it restricts the search to a straight path that may poorly approximate the feasible region. To illustrate this limitation, the benchmark problem HS-19 from the Hock and Schittkowski test set[17] is used to demonstrate that an arc-search strategy, which follows curved paths better aligned with the geometry of the constraints, can provide a more effective alternative.

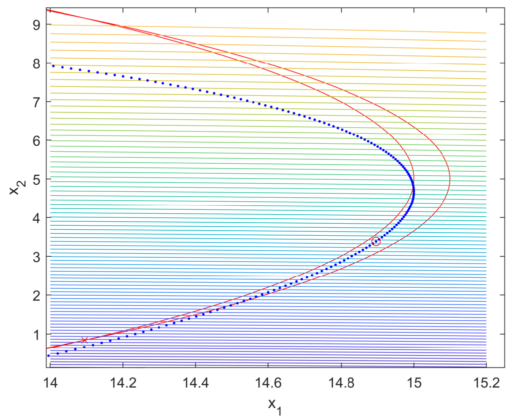

Figure 5. The arc used for searching optimizer at current iterate of Problem (9).

$$\begin{array}{rcl} \min & : & f(\mathbf{x}) = (x_1 - 10)^3 + (x_2 - 20)^3 \\ \text{s.t.} & : & (x_1 - 5)^2 + (x_2 - 5)^2 - 100 \geq 0 \\ & & -(x_2 - 5)^2 - (x_1 - 6)^2 + 82.81 \geq 0 \\ & & 13 \leq x_1 \leq 100 \\ & & 0 \leq x_2 \leq 100 \end{array} \quad (9)$$

For this problem, the last 4 boundary inequalities are redundant. The feasible region is illustrated in Figure 4, lying between two red curves. The contour lines represent the level sets of the objective function, which decrease in the top-down direction. The optimal solution is at the intersection of the two red curves, marked with a red 'x'. For an iterate within the feasible region, searching along a descent line segment is not as effective as following a curved path. In particular, an arc-search strategy—such as the elliptical arc shown in Figure 5—better conforms to the geometry of the feasible region and can lead to a more efficient search toward the optimizer.

For general nonlinear optimization problems (8) (the problem (9) illustrated in Figure refarcApp is a special case), it is shown by Yang[12] that the arc (represented in blue) passing through the current iterate (marked with a red 'o') can be constructed systematically and used to guide the search for

‡For LISA, the problem is nonlinear and nonconvex, and the suitability of IPM for this problem is discussed by Yang et al[15].

the optimizer. The advantages of employing arc-search within an interior-point framework for LISA optimal orbit design were analyzed in an internal report[15]. The algorithm was subsequently formalized by Yang[12], where its convergence to the optimizer was established under mild assumptions[§]. An optimization tool implementing the algorithm has been developed by the author[12]. This tool supports the computation of first- and second-order derivatives for the objective and constraint functions via automatic differentiation[¶]. The computational efficiency and effectiveness of the algorithm have been validated through a series of numerical experiments involving thousands of nonlinear and nonconvex optimization problems[19]. The results were compared with those obtained using Matlab `fmincon` function, which implements two widely used algorithms: a line-search interior-point method and a sequential quadratic programming (SQP). The comparisons indicate that the arc-search interior-point method consistently outperforms `fmincon` function under both algorithmic settings [19].

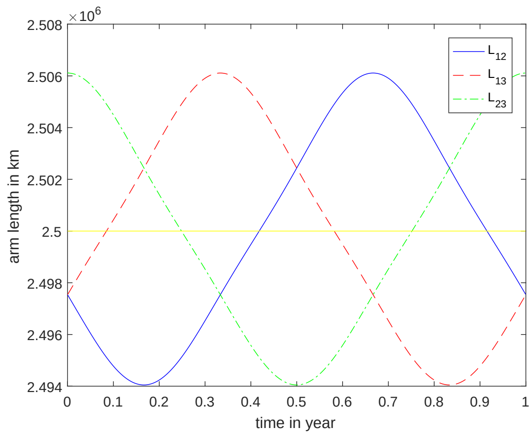

Figure 6. Inter-spacecraft distances over one orbital period (one year) for the optimal orbit, using 629 sampling points.

Optimal orbit design assuming identical e_k and i_k for all spacecraft k

As discussed in the Introduction section, each LISA spacecraft orbit can be assumed to be elliptical, with its size and shape determined solely by the semi-major axis a and eccentricity e. Since the constellation period must match the Earth's orbital period, we set $a = R$, where R denotes the orbital radius of LISA constellation's virtual center. Each spacecraft orbit is inclined with respect to the ecliptic plane by an angle i. As the right ascension of the ascending node and the argument of aphelion are implicitly defined in Figure 1, only e and i remain as independent design variables to be optimized. The parameter δ is implicitly determined by i and is therefore redundant. We formulate the orbit design problem as an optimization problem that directly selects the optimal values of i and e to minimize the deviation of the inter-spacecraft distances from a prescribed constant, subject to the constraints defined in (3),(4), and (5).

Let $T = \frac{2\pi}{\Omega}$ be the orbital period the three spacecraft. For $0 = t_0 < t_1 < \ldots < t_{n-1} < t_n = T$, the desired distance between spacecraft i and j (for $1 \le i < j \le 3$) is $\ell_{i,j} = 2{,}500{,}000$ km, and denote $\Delta X_{i,j}(k) = X_i(t_k) - X_j(t_k)$, $\Delta Y_{i,j}(k) = Y_i(t_k) - Y_j(t_k)$, and $\Delta Z_{i,j}(k) = Z_i(t_k) - Z_j(t_k)$. Then, the distance deviation between spacecraft i and j at time t_k from the desired distance is given by

$$d_{i,j}(t_k) = \sqrt{\Delta X_{i,j}(k)^2 + \Delta Y_{i,j}(k)^2 + \Delta Z_{i,j}(k)^2} - \ell_{i,j}. \tag{10}$$

Our objective is to minimize the cumulative distance deviation in (10) for all t_k, subject to satisfying the orbital constraints in (3), (4), and (5) for all t_k. In addition, we impose box constraints on e and i to ensure physical feasibility and to improve the convergence behavior. Therefore, the optimization problem can be written as follows.

$$\begin{array}{ll}
\min & \sum_{t_k=0,\ldots,T} \sum_{1\le i<j\le 3} d_{i,j}^2(t_k) \\
\text{s.t.} & E_1(t_k) + e\sin(E_1(t_k)) = \Omega t_k \\
& E_2(t_k) + e\sin(E_2(t_k)) = \Omega t_k - \frac{2\pi}{3} \\
& E_3(t_k) + e\sin(E_3(t_k)) = \Omega t_k - \frac{4\pi}{3} \\
& X_1(E_1(t_k)) = a(\cos(E_1(t_k)) + e)\cos(i) \\
& Y_1(E_1(t_k)) = a\sqrt{1-e^2}\sin(E_1(t_k)) \\
& Z_1(E_1(t_k)) = a(\cos(E_1(t_k)) + e)\sin(i) \\
& X_2(t_k) = X_1(E_2(t_k))\cos\left(\frac{2\pi}{3}\right) - Y_1(E_2(t_k))\sin\left(\frac{2\pi}{3}\right) \\
& Y_2(t_k) = X_1(E_2(t_k))\sin\left(\frac{2\pi}{3}\right) + Y_1(E_2(t_k))\cos\left(\frac{2\pi}{3}\right) \\
& Z_2(t_k) = Z_1(E_2(t_k)) \\
& X_3(t_k) = X_1(E_3(t_k))\cos\left(\frac{4\pi}{3}\right) - Y_1(E_3(t_k))\sin\left(\frac{4\pi}{3}\right) \\
& Y_3(t_k) = X_1(E_3(t_k))\sin\left(\frac{4\pi}{3}\right) + Y_1(E_3(t_k))\cos\left(\frac{4\pi}{3}\right) \\
& Z_3(t_k) = Z_1(E_3(t_k)) \\
& 0 = \Omega t_0 < \Omega t_1 < \ldots < \Omega t_{n-1} < \Omega t_n = 2\pi \\
& 0 \le e \le 0.01, \quad 0 \le i \le \pi/6
\end{array} \tag{11}$$

where i and e are independent variables, and $0 \le \Omega t_k \le 2\pi$. For fixed i and e, the eccentric anomalies E_1, E_2, and E_3 of spacecraft 1, 2, and 3 are functions of time t_k. Consequently, the Cartesian coordinates of the i-th spacecraft X_i, Y_i, and Z_i are functions of $E_i(t_k)$ for $i = 1, 2, 3$.

Setting the number of sampling points $n = 629$ (corresponding to a uniform discretization with step size of 0.01 over the interval $[0, 2\pi]$), and starting from a feasible point $(e, i) = (0.0047975, 0.008315)$ (obtained via a trial-and-error procedure near the values derived from NKDV/DNKV methods), we obtained the optimal solution after 14 iterations in 8.2937 seconds (with a converge criterion of the norm of KKT conditions smaller than 10^{-8}):

$$(e^*, i^*) = (0.004824385965325, 0.008355663130457).$$

The inter-spacecraft distances are computed using (3), (4), and (5). The results are presented in Figure 6,

---

[§]The algorithm is an improved version of the arc-search infeasible interior-point algorithm by Yamashita et al[18]

[¶]Details about automatic differentiation can be found in the book of Nocedal and Wright[16].

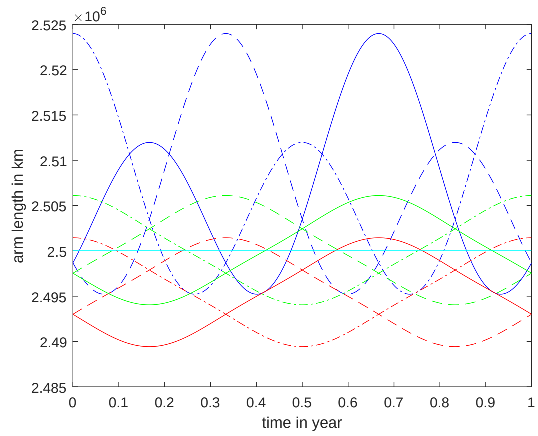

Figure 7. Inter-spacecraft distances comparison of all three orbit designs, using 629 sampling points.

where the horizontal line represents the desired distance between any spacecraft pair. The solid line denotes the distance variation between spacecraft 1&2, the dashed line corresponds to spacecraft 1&3, and the dash-dotted line corresponds to spacecraft 2&3.

A quantitative comparison of orbit errors for the three designs is summarized in Table 1. These errors degrade LISA's performance due to their impact on the signal-to-noise ratio[20], time-delay interferometry (TDI)[21], and unmodeled perturbation forces[7,22]. The results indicate that both the NKDV and optimal designs improve upon the DNKV design, and that the optimal design further improves upon the NKDV design.

A graphic orbit comparison of all three designs is shown in Figure 7, where the cyan line represents the desired distance. The blue, red, and green lines correspond to DNKV, NKDV, and optimal orbit designs, respectively. For each design, the solid, dashed, and dash-dotted lines denote the distances between spacecraft pair $(1,2)$, $(1,3)$, and $(2,3)$, respectively. The distance variation of DNKV design is approximately 2.8789×10^4 km, the distance variation of NKDV design is approximately 1.2×10^4 km, which is comparable to that of the optimal design. However, the latter is centered around 2.5×10^6 km, whereas the former is not. When the perturbation forces are considered in a higher-fidelity model[22], maintaining centering around 2.5×10^6 km becomes important.

Optimal orbit design assuming different e_k and i_k for all spacecraft k

In this design, we assume that the eccentricity and inclination of spacecraft k are e_k and i_k for $k = 1, 2, 3$. We investigate whether the additional degrees of freedom can lead to an improved optimal configuration. For this purpose, Kepler's equation for each spacecraft is given by

$$E_k + e_k \sin(E_k) = \Omega t - (k-1)\frac{2\pi}{3}, \quad k = 1, 2, 3. \quad (12)$$

Accordingly, the orbital coordinates in a common reference frame are modified as

$$\tilde{X}_k(E_k) = a(\cos(E_k) + e_k)\cos(i_k), \quad (13a)$$
$$\tilde{Y}_k(E_k) = a\sqrt{1-e_k^2}\sin(E_k), \quad (13b)$$
$$\tilde{Z}_k(E_k) = a(\cos(E_k) + e_k)\sin(i_k), \quad (13c)$$

for $k = 1, 2, 3$. The final ecliptic coordinates of the spacecraft are then obtained by rotating each orbit by $2\pi(k-1)/3$ about the Z-axis:

$$\begin{aligned} X_k &= \tilde{X}_k(E_k)\cos\left(\frac{2\pi}{3}(k-1)\right) \\ &\quad -\tilde{Y}_k(E_k)\sin\left(\frac{2\pi}{3}(k-1)\right), \quad (14a) \end{aligned}$$

$$\begin{aligned} Y_k &= \tilde{X}_k(E_k)\sin\left(\frac{2\pi}{3}(k-1)\right) \\ &\quad +\tilde{Y}_k(E_k)\cos\left(\frac{2\pi}{3}(k-1)\right), \quad (14b) \end{aligned}$$

$$Z_k = \tilde{Z}_k(E_k), \quad (14c)$$

for $k = 1, 2, 3$. Combining all above formulas yields the optimization problem:

$$\begin{array}{ll} \min & \sum_{t_k=0,\ldots,T} \sum_{1\le i<j\le 3} d_{i,j}^2(t_k) \\ \text{s.t.} & E_1(t_k) + e_1\sin(E_1(t_k)) = \Omega t_k \\ & E_2(t_k) + e_2\sin(E_2(t_k)) = \Omega t_k - \frac{2\pi}{3} \\ & E_3(t_k) + e_3\sin(E_3(t_k)) = \Omega t_k - \frac{4\pi}{3} \\ & X_1(E_1(t_k)) = a(\cos(E_1(t_k)) + e_1)\cos(i_1) \\ & Y_1(E_1(t_k)) = a\sqrt{1-e_1^2}\sin(E_1(t_k)) \\ & Z_1(E_1(t_k)) = a(\cos(E_1(t_k)) + e_1)\sin(i_1) \\ & \tilde{X}_2(E_2(t_k)) = a(\cos(E_2(t_k)) + e_2)\cos(i_2) \\ & \tilde{Y}_2(E_2(t_k)) = a\sqrt{1-e_2^2}\sin(E_2(t_k)) \\ & \tilde{Z}_2(E_2(t_k)) = a(\cos(E_2(t_k)) + e_2)\sin(i_2) \\ & \tilde{X}_3(E_3(t_k)) = a(\cos(E_3(t_k)) + e_3)\cos(i_3) \\ & \tilde{Y}_3(E_3(t_k)) = a\sqrt{1-e_3^2}\sin(E_3(t_k)) \\ & \tilde{Z}_3(E_3(t_k)) = a(\cos(E_3(t_k)) + e_3)\sin(i_3) \\ & X_2 = \tilde{X}_2(E_2)\cos\left(\frac{2\pi}{3}\right) - \tilde{Y}_2(E_2)\sin\left(\frac{2\pi}{3}\right) \\ & Y_2 = \tilde{X}_2(E_2)\sin\left(\frac{2\pi}{3}\right) + \tilde{Y}_k(E_k)\cos\left(\frac{2\pi}{3}\right) \\ & Z_2 = \tilde{Z}_2(E_2) \\ & X_3 = \tilde{X}_3(E_3)\cos\left(\frac{4\pi}{3}\right) - \tilde{Y}_3(E_3)\sin\left(\frac{4\pi}{3}\right) \\ & Y_3 = \tilde{X}_3(E_3)\sin\left(\frac{4\pi}{3}\right) + \tilde{Y}_k(E_3)\cos\left(\frac{4\pi}{3}\right) \\ & Z_3 = \tilde{Z}_3(E_3) \\ & 0 = \Omega t_0 < \Omega t_1 < \ldots < \Omega t_{n-1} < \Omega t_n = 2\pi \\ & 0 \le e \le 0.01, \quad 0 \le i \le \pi/6 \end{array} \quad (15)$$

Starting from the following feasible point

$$\begin{aligned} & (e_1, i_1, e_2, i_2, e_3, i_3,) \\ = \; & (0.0047975, 0.008315, 0.0047975, 0.008315, 0.0047975, 0.008315), \end{aligned}$$

after 14 iteration, an optimal solution was obtained in 9.2381 second

$$\begin{aligned} & (e_1, i_1, e_2, i_2, e_3, i_3,) \\ = \; & (0.0048244, 0.0083556, 0.0048243, 0.0083556, 0.0048243, 0.0083556), \end{aligned}$$

Table 1. Statistic orbit error for three differenct designs.

Error measurements	Spacecraft pair	DNKV design	NKDV design	Optimal design
Peak-to-peak	(1,2)	25391 km	12018 km	12061 km
	(1,3)	25391 km	12018 km	12061 km
	(2,3)	25414 km	12040 km	12084 km
Maximum instantaneous deviation	(1,2)	20572 km	10568 km	6109.9 km
	(1,3)	20572 km	10568 km	6109.8 km
	(2,3)	20595 km	10568 km	6132.2 km
Root-mean-square	(1,2)	2.5050e+6 km	2.4954e+6 km	2.5000e+6 km
	(1,3)	2.5050e+6 km	2.4954e+6 km	2.5000e+6 km
	(2,3)	2.5050e+6 km	2.4955e+6 km	2.5000e+6 km
Standard deviation	(1,2)	7851.8 km	3994.0 km	4008.6 km
	(1,3)	7851.8 km	3994.0 km	4008.6 km
	(2,3)	7865.0 km	3998.1 km	4012.8 km
Standard error of the mean	(1,2)	313.0723 km	159.2509 km	159.8333 km
	(1,3)	313.0702 km	159.2509 km	159.8333 km
	(1,3)	313.5978 km	159.4160 km	160.0024 km

which is the same result we obtained in the previous section. Starting from some random initial points near the above optimal solution, we obtained the same result. This suggests that the optimal solution of (11) is likely a locally optimal solution of (15) within a relatively large neighborhood, whereas De Marchi et al[1], Hughes[5], and Nayak et al[3] have not demonstrated this property. Since problem (11) is simpler than problem (15), solving (11) is computationally more efficient than solving (15). Finally, the optimization algorithm proposed in this paper can be applied to higher-fidelity model[22], and may yield improved formation orbit designs due to its algorithmic advantages analyzed by Yang[12]. This extension is left as a topic for future research.

Extension to n spacecraft in formation flight

We have discussed the solution of 3 spacecraft in formation flying. The method discussed in Section can be readily extended to the case of $n \geq 4$ spacecraft in formation flying. The key idea is to use (2) and (3) to represent the orbit of spacecraft 1. Then the orbit presentation for the k-th $(k = 2, \ldots, n)$ spacecraft can be obtained by rotating the orbit of spacecraft 1 by $360(k-1)/n$ about the center of the coordinate system (the Sun, see Figure 1). Following the same procedure as previously discussed in this section, we obtain an optimization problem similar to (11), and the optimization algorithm/tool developed by this author[12] can be used to solve the general case.

Conclusions

The LISA orbit design problem is formulated as a nonlinear and nonconvex optimization problem using the exact nonlinear Keplerian orbital equations. The solution of this higher-fidelity model provides a more accurate optimal configuration, leading to a smaller mean deviation of the inter-spacecraft distance from the prescribed value compared with the existing methods. It is well known that nonlinear and nonconvex optimization problems are challenging to solve, therefore, a recently proposed and numerically validated arc-search interior-point algorithm is employed. The resulting solution minimizes the deviation of inter-spacecraft distance from a prescribed constant, thereby reducing the Doppler shift and breathing angle effects in the measurement of gravitational waves. Since the proposed algorithm has been proven to converge to an optimizer, and the numerical results are consistent with the theoretical analysis, we expect the method can be extended to other higher-fidelity models for LISA formation flying orbit design.

Acknowledgements

This work is supported in part by NASA's IRAD 2023 fund SSMX22023D. The author thanks Dr. Pritchett at NASA's Goddard Space Flight Center for his valuable comments and suggestions, which helped improve the presentation of the paper. The author is also grateful to the anonymous reviewers and the associate editor for their constructive comments, which contributed to the preparation of the revised version.

Data availability statement

The Matlab code that is used to generate the result is available upon reasonable request.

Conflict of interest

The author declares no conflict of interest.

References

1. Dhurandhar SV, Nayak KR, Koshti S, et al. Fundamentals of the LISA stable flight formation. *Classical and Quantum Gravity* 2005; 22, 481–487.
2. De Marchi FG, Pucacco G, and Bassan F. Optimizing the Earth–LISA 'rendezvous'. *Classical and Quantum Gravity* 2012; 29 035009.
3. Nayak KR, Koshti S, Dhurandhar SV et al. On the minimum flexing of LISA's arms. *Classical and Quantum Gravity* 2006; 23, 1763–1778.
4. Amato JC (2019) *Flying in formation: The orbital dynamics of LISA's three spacecraft*, Am. J. Phys. 87 (1), 18-23.

5. Hughes SP Preliminary optimal orbit design for laser interferometer space antenna. *25th Annual AAS Guidance and Control Conference*, Breckenridge CO, Feb. 2002.
6. Clohessy W and Wiltshire R. Terminal guidance system for satellite rendezvous. *Journal of Astronautical Sciences* 1960; 27(9), 653–678.
7. Martens W and Joffre E. Trajectory Design for the ESA LISA Mission. *J Astronaut Sci* 2021; 68, 402–443.
8. Bayle J-B, Hees A, Lilley M et al. LISA Orbits URL https://ui.adsabs.harvard.edu/abs/2022zndo...7700361B/abstract, 2022.
9. Yang Y. *Spacecraft Modeling, Attitude Determination, and Control: Quaternion-Based Approach*, 2nd Edition, CRC Press, 2025.
10. Danilova M, Dvurechensky P, Gasnikov A et al. Recent Theoretical Advances in Non-Convex Optimization. *High-Dimensional Optimization and Probability* Springer, 2022; pp. 79–163.
11. Wächter A and Biegler LT. Line search filter methods for nonlinear programming: motivation and global convergence. *SIAM Journal on Optimization* 2005; 16(1), 1-31.
12. Yang Y. An arc-search interior-point algorithm for nonlinear constrained optimization. *Computational Optimization and Applications* 2025; 90, pp. 969–995.
13. Vallado DA. Fundamentals of astrodynamics and applications. *Springer Science & Business Media* 2001; pp. 310-316.
14. Wie B. Space Vehicle Dynamics and Control. *AIAA Education Series* AIAA Inc., Reston 1998.
15. Yang Y, Pritchett R, Hatten N. An infeasible interior-point arc-search algorithm for spacecraft trajectory optimization. *INFORMS Optimization* 2024; Huston, March 22-24.
16. Nocedal J and Wright SJ. Numerical Optimization. *Springer* New York 2006.
17. Hock W and Schittkowski K. Test examples for nonlinear programming codes. *in Lecture Notes in Economics and Mathematical Systems* volume 187, Springer 1981.
18. Yamashita M, Iida E, and Yang Y. An infeasible interior-point arc-search algorithm for nonlinear constrained optimization. *Numerical Algorithms* 2022; 12, pp. 781–798.
19. Yang Y, Le Q, and Weintraub IE. Combining reinforcement learning with arc-search interior-point method for path planning' *arXiv*:2606.07920v2 [math.OC] 09 Jun 2026.
20. Katz ML, Jean-Baptiste B, Chua JKA. Assessing the data-analysis impact of LISA orbit approximations using a GPU-accelerated response model. *Physical Review D* 2022; 106, 103001.
21. Page J and Littenberg T. Bayesian time delay interferometry for orbiting LISA: Accounting for the time dependence of spacecraft separations. *Physical Review D* 2023; 108, 044065.
22. Joffre E, Wealthy D, Fernandez I et al. LISA: Heliocentric formation design for the laser interferometer space antenna mission. *Adavnces of Space Research* 2021; 67, pp. 3868-3879.